Journal Pre-proof


# Exploring the global thunderstorm influence on the fair weather electric field in Buenos Aires

Yasmin R. Velazquez, M. Gabriela Nicora, Vito S. Galligani, E.A. Wolfram, P.V. Salio, Raul L. D'Elia

PII: S0169-8095(23)00579-3

DOI: https://doi.org/10.1016/j.atmosres.2023.107182

Reference: ATMOS 107182

To appear in: *Atmospheric Research*

Received date: 24 July 2023

Revised date: 16 November 2023

Accepted date: 12 December 2023

Please cite this article as: Y.R. Velazquez, M.G. Nicora, V.S. Galligani, et al., Exploring the global thunderstorm influence on the fair weather electric field in Buenos Aires, *Atmospheric Research* (2023), https://doi.org/10.1016/j.atmosres.2023.107182

This is a PDF file of an article that has undergone enhancements after acceptance, such as the addition of a cover page and metadata, and formatting for readability, but it is not yet the definitive version of record. This version will undergo additional copyediting, typesetting and review before it is published in its final form, but we are providing this version to give early visibility of the article. Please note that, during the production process, errors may be discovered which could affect the content, and all legal disclaimers that apply to the journal pertain.

© 2023 Published by Elsevier B.V.

Journal Pre-proof

# Exploring the Global Thunderstorm Influence on the Fair Weather Electric Field in Buenos Aires

Yasmin R. Velazquez[a,b,d], M. Gabriela Nicora[a,b], Vito S. Galligani[b,c,d], E. A. Wolfram[a,b,e], P. V. Salio[b,c,d], Raul L. D'Elia[a]

[a]*Centro en Laseres y Aplicaciones (CEILAP) CITEDEF and UNIDEF (MINDEF-CONICET), , Vicente Lopez, , Buenos Aires, Argentina*

[b]*CNRS – IRD – CONICET – UBA. Instituto Franco-Argentino para el Estudio del Clima y sus Impactos (IRL 3351 IFAECI), , Ciudad Autonoma de Buenos Aires, , Ciudad Autonoma de Buenos Aires, Argentina*

[c]*CONICET – Universidad de Buenos Aires. Centro de Investigaciones del Mar y la Atmosfera (CIMA), , Ciudad Autonoma de Buenos Aires, , Ciudad Autonoma de Buenos Aires, Argentina*

[d]*Universidad de Buenos Aires, Facultad de Ciencias Exactas y Naturales, , Ciudad Autonoma de Buenos Aires, , Ciudad Autonoma de Buenos Aires, Argentina*

[e]*Direccion de Redes de Observacion del SMN C1425GBE, , Ciudad Autonoma de Buenos Aires, , Ciudad Autonoma de Buenos Aires, Argentina*

Journal Pre-proof

**Abstract**

The Global atmospheric Electric Circuit (GEC) sustains the fair weather (FW) electric field, or potential gradient (PG). In this article, we analyze PG measurements recorded between 2017 and 2021 at the Instituto de Investigaciones Científicas y Técnicas para la Defensa (CITEDEF) in Buenos Aires, Argentina, to calculate the daily PG (FW) curve and examine

*Email address:* yasmin_rv@outlook.com (Yasmin R. Velazquez)

whether local PG measurements capture the GEC signal. With the aim of supporting future common methodologies that do not rely on meteorological data for FW identification - and hence aid inter-comparisons, we rely on previously developed statistical methodologies to propose a FW selection based on the absolute deviation from the median of the data series. Using this methodology we filtered FW days and showed that the local PG (FW) curve had a significant correlation of 0.83 with the Carnegie curve. In order to test the extent to which the local daily PG (FW) curve captures the global thunderstorm signal, the area of thunderstorms was calculated at both global and regional scales using data from the Thunder Hour Database (http://thunderhours.earthnetworks.com). The PG (FW) curve was shown to have a good correlation with the daily median variation of the global thunderstorm area on both annual and quarterly scales. Additionally, the analysis of coincident aerosol optical thickness (AOD) measurements by the AERONET network and temperature observations helped to conclude that local effects such as pollution from a near highway are not dominating the PG (FW) curve behaviour. Both analyses allowed us to conclude that the GEC signal can be detected in Buenos Aires.

Highlights

- The daily PG curve (FW) in Buenos Aires has a correlation of 0.83 with the Carnegie curve with 95% confidence.
- The daily PG (FW) curve in Buenos Aires has a seasonal variation that accompanies the global changes of thunderstorm areas.
- Local effects such as pollution from a near highway are not dominating the PG (FW) curve behaviour.

Journal Pre-proof

*Keywords:* potential gradient, electric field, fair weather, Argentina, Global atmospheric electric circuit

# 1. Introduction

The Global Atmospheric Electric Circuit (GEC) is a complex system that can be affected in the lower atmosphere by thunderstorms, shower clouds, cosmic rays and aerosols, among others (Kumar et al., 2018; Victor et al., 2020). In the middle/upper atmosphere, between the stratosphere and the mesosphere, phenomena like transient luminous events also affect the GEC (Victor et al., 2020). The GEC is a circuit that integrates processes in both the neutral atmosphere and the ionosphere. In the upper layers, the ionospheric potential of the GEC can be affected to a greater or lesser extent by solar events, lightning, and sprites(Rycroft et al., 2008).

Electrical activity is not homogeneously distributed across the planet. Blakeslee et al. (2014) compared the number of storms observed over the continent and the ocean, and found that over land, more than twice as many storms occur compared to those over the oceans. In particular, a continental maximum occurs in the northern hemisphere (NH) summer quarter of JJA, where approximately 3.5 times as many storms are observed over land. The quarter with the lowest number of storms observed over the continent is the DJF quarter. This predominance in the number of storms in the JJA quarter is due to the larger continental area in the northern hemisphere. In terms of thunderstorms, a similar situation to the number of storms is observed; the oceanic regions contribute between 10% and 14% of the total, showing continental predominance (Blakeslee et al., 2014; Mezuman et al., 2014).

Measurements of the atmospheric potential gradient (PG, defined as minus the vertical

Journal Pre-proof

electric field, $-E$) have been used to monitor the GEC and analyze the variability of the lower atmospheric electricity. PG has been tightly linked to the study of atmospheric electricity since 1750, when Canton (1753) confirmed the persistence of PG even in the absence of thunderstorms. Between 1909 and 1929, the Carnegie Institution made hourly measurements of PG around the oceans and showed that the mean daily variation of PG on fair weather (FW) days, hereafter the PG (FW) diurnal curve, did not depend on the geographical position at which the measurements were taken. This study resulted in the global diurnal climatological variation of FW conditions, known as the Carnegie curve (Israel, 1973; Harrison, 2004). The Carnegie curve is characterised by a minimum around 3 UTC and a maximum around 19 UTC. Similarly, local PG (FW) curves around the world have been analyzed to monitor the GEC (Kamogawa et al., 2015; Harrison and Nicoll, 2018; Lucas et al., 2017; Tacza et al., 2021, Velazquez, 2021; Yaniv et al., 2016). Whipple (1929) found that the daily variation of the global thunderstorm area has a very high correlation with the Carnegie curve, which was found in subsequent studies to be due to the fact that this PG signal is maintained across the GEC by thunderstorm and electrified shower clouds (Rycroft et al., 2000; Liu et al., 2010; Mach et al., 2011; Williams and Mareev, 2014).

The FW conditions used in the Carnegie Institution's measurements were selected using only positive PG values and no presence of hydrometeors (Sverdrup, 1944). Subsequently, the need to identify the meteorological conditions associated with FW became important to analyse their associated PG values. Different studies have defined FW conditions on the basis of either meteorological parameters (i.e., the meteorological approach) or the behaviour of PG values (i.e., the statistical approach). The magnitude of PG on days with FW is usually 100 $Vm^{-1}$ or less. The days that are not classified as FW days are defined as Disturbed Weather (DW) days and the magnitude of PG on these days can reach 1000 $Vm^{-1}$ or more. Kamogawa et al. (2015) defined

FW days as days with no clouds directly above Mt. Fuji, while Harrison and Nicoll (2018), Gurmani et al. (2018) and Afreen et al. (2022) included thresholds for wind speed, cloud cover and the absence of hydrometeors at the location of the PG measurement. Lucas et al. (2017) and Nicoll et al. (2019) among others discussed alternative statistical methods for stations without conventional meteorological measurements. Lucas et al. (2017) proposed to use thresholds of the deviation from the PG median as a method to identify FW conditions, in order to avoid using arbitrary values to define FW and to avoid data contaminated by outliers as it can occur when using the mean PG for example - another commonly used approach. Instead, in Nicoll et al. (2019) for example, PG (FW) values are identified as those positive PG values that are within 80% of the cumulative distribution of PG values. Conversely, for sites where pollution levels and dominant wind directions have been documented to cause an increase or decrease in PG, it may be necessary to exclude those directions that act as a source (Frank-Kamenetsky et al., 1999).

There are phenomena that can obscure the GEC signal. One of these phenomena is the so-called sunrise effect. At dawn, increased turbulence in the boundary layer transports upward positive charges accumulated near the surface. This transport of charges over the gauge can result in an increase in PG (Lucas et al., 2017; Afreen et al., 2022). The same turbulence that occurs at dawn also transports aerosols. This increase in the amount of aerosols in the air can lower the conductivity of the atmosphere resulting in an increase in PG (Anisimov et al., 2018). Pollution, a type of anthropogenic aerosol, has an extra contribution in that it is maximised during peak traffic hours. For this reason, there are sites where PG values reach their maximum values during hours of high vehicular traffic (Tacza et al., 2020). Topography can introduce other types of more complex interactions that also alter PG values such as mountain circulations or the formation of a sea of clouds (Kamogawa et al., 2015; Yaniv et al., 2017; Afreen et al., 2022).

Journal Pre-proof

Tacza et al. (2021) analysed the measuring station located in Argentina for a series of 9 years. They found a correlation of 0.85 and 0.95 between the Carnegie curve and the daily mean PG (FW) curves at seasonal and annual scales respectively, with a maximum in the winter months (JJA). In Velazquez (2021), the daily mean PG (FW) curve in Buenos Aires, Argentina (see the measurement site in Figure 1.a – red star) was calculated using 2 different methodologies to select the FW days. In Figure 3.9 of that work, a strong correlation between the two methodologies is observed. With both methods, the PG (FW) curves were calculated and showed good correspondence with the daily pattern of the Carnegie curve. As for seasonal variations, a pattern consistent with seasonal changes in global lightning was observed. Velazquez (2021) further demonstrated that it is not always possible to assume that the number of FW days is greater than the number of DW days, as assumed in Tacza et al. (2018), as it is highly dependent on local conditions.

Given the usefulness of PG observations for various applications, the motivation of this work is to contribute to the analysis of local PG observations in order to improve the characterisation of the atmosphere from an electrical point of view. The aim of this work is to explore the global thunderstorm influence on the FW electric field in Buenos Aires, more specifically at the Institute de Investigaciones Científicas y Técnicas para la Defensa (CITEDEF, 34° 19.62’ S, 58° 22.40’ W) or the Buenos Aires Station hereafter, as it will be known from now on. In order to achieve this, a preliminary analysis of the effects of pollution and the sunrise effect on the PG (FW) curve is first conducted.

To obtain the PG diurnal curve (FW) and compare it with the Carnegie curve and two other continental stations, a period of 5 years – 2017 to 2021 inclusive – was studied. This exercise allows, among other things, to determine the representativeness of the local signal for monitoring

the GEC. There are a large number of similar studies examining daily mean PG curves under FW conditions (Lucas et al., 2017; Nicoll et al., 2019; Tacza et al., 2021; Afreen et al., 2022). However, one factor that complicates the comparison is the lack of a clear and documented methodology for selecting FW days that can be applied globally. This paper will rely on the methodology used in Lucas et al. (2017) to propose a methodology to select FW days that is not affected by outlier PG values (Buzás et al., 2022). We seek to analyse the impact of the global and regional thunderstorm area and its correlation with the locally observed PG (FW) signal at Buenos Aires Station, to deepen the understanding of the impact of the GEC at the study site. For this purpose, the aerosol optical thickness (AOD) and temperature data will be analysed to understand the importance of local effects in the local PG curve (FW). The AOD is used as a proxy for aerosol concentration (e.g., Tacza et al. (2020))

Following the reasoning behind this paper, this document will be organised as follows: Section 2 describes the data used. Section 3 presents the methodology applied for the selection of FW days as well as for the calculation of the daily PG (FW) curve, average daily temperature curve, average daily AOD curve and thunderstorm areas. In section 4, the results obtained will be shown. Finally, the conclusions of the work will be presented in section 5.

Journal Pre-proof

# 2. Data

## *2.1. Potential Gradient*

Figure 1.a shows the geographical location of the Buenos Aires Station (red star) where a Campbell Scientific CS110 PG meter is installed. It is located in Greater Buenos Aires, one of the largest metropolitan areas in Latin America. The population of this large megalopolis is around 3 million inhabitants in the city of Buenos Aires and 17 million in the 24 surrounding districts

(INDEC, 2022). In contrast to other Latin American cities, the city of Buenos Aires and the surrounding area is located on a plain on the banks of the Río de la Plata, which flows into the sea. This allows a better ventilation of pollutants than in other Latin American cities (Bogo et al., 1999). The instrument is located at a height of 2 m above the ground (20 m above sea level). The measuring range is ± 21000 $Vm^{-1}$ with a time resolution of 5 s. The sensor is mounted on the roof of the institution where other instruments are operating. At a distance of 3 m from one side of the building there are some trees, unlike the other 3 sides (see Figure 1.b). It was decided to place the instrumentation on the roof in order to have better control of the condition of the trees due to the presence of animals that may be roaming around inside the building. Its proximity to some trees could affect the long-term variation of the PG variable (Williams et al., 2005; Buzás et al., 2021).

The variable PG has been measured continuously in the institution from 2017 until the end of December 2021 the data are available at `http://hdl.handle.net/11336/217041`. Its location is about 500 metres away from a highway, so the PG data may be affected by pollution. It is also worth noting the existence of a large area of parks in the surrounding area should also be highlighted, allowing a better dilution of pollutants.

The local PG curve is compared to other continental stations as well as the Carnegie curve. The PG values for the Carnegie curve are taken from Harrison (2004). The CASLEO PG (FW) continental curve was provided by J. Tacza at El Leoncito, Argentina, as calculated in Tacza et al. (2021). Finally, the Mitzpe Ramon PG curve (FW) named after its measurement site (Mitzpe Ramon, Israel) has been taken from Yaniv et al. (2016). Note that the criteria for choosing FW days is different and that the location of these sites offer very different environments.

## *2.2. Atmospheric optical depth and temperature*

Journal Pre-proof

The Buenos Aires station has many other atmospheric instruments. Among them is the sun photometer belonging to the Aerosol Robotic Network (AERONET). This passive remote sensing instrument is responsible for sensing the properties of aerosols, water vapour and ozone in the entire atmospheric column. This instrument works in 8 bands between 340 nm and 1020 nm. The extinction in some of the bands are used for the calculation of the aerosol optical thickness (AOD) by this network. The uncertainties in the AOD calculation range from ±0.01 in the infrared to ±0.02 in the ultraviolet. Another instrument that is responsible for sensing the state of the atmosphere is the temperature sensor that is part of a Campbell scientific automatic station. Like the electric field meter, the temperature sensor stores data every 5 seconds.

### *2.3. Thunder hours data*

DiGangi et al. (2021) constructed a thunder hour database using the Earth Networks Global Lightning Detection Network (ENGLN), which combines ground-based instruments from the Earth Networks Total Lightning Network (ENTLN) and the World Wide Lightning Location Network (WWLLN). These networks have been shown to have a high detection efficiency (Lapierre et al., 2021). The DiGangi et al. (2021) database has a resolution of 0.05°x0.05° in latitude and longitude. In the DiGangi et al. (2021) database, thunder hour is defined as an hour during which at least two lightning discharges are detected within 15 km of a given point. The use of this database allows thunderstorms with a lower lightning rate to be included. In Section 3.2, we present the methodology used to calculate thunderstorm area.

## 3. Methodology

Journal Pre-proof

### *3.1. Study of FW Days*

A baseline analysis with all data (2017-2021) is presented first to understand the general behaviour of the PG database. As a second step, the days fulfilling a FW condition were selected. Given the impossibility of generalising PG thresholds for FW conditions globally and the need for a robust statistical approach in the absence of meteorological data, we propose to define the absolute deviation from the median (MAD) as they do in the work of Lucas et al. (2017):

$$MAD = median(|X_i - median(X)|) \quad (1)$$

where $X_i$ is observation number i, and median( $X$ ) is the median of the whole series. The statistical approach we propose is to filter FW days with absolute values of PG greater than 5 MAD with respect to the median of the complete series in order to eliminate the extreme values. Once the days with FW conditions were obtained, the daily mean PG (FW) curve was calculated. For this purpose, averages were taken for each of the 1440 minutes of the day. In addition, the standard deviation of the daily FW curve was calculated. The series of FW days was also used to calculate daily variations on a quarterly and annual scale.

Note that the PG data could not have an absolute calibration correction as done in other studies like Gurmani et al. (2018). For this reason, PG (FW) curves will not be presented in terms of their absolute values. They will be shown in terms of the percentage of their mean value. This standardisation will also be applied to the standard deviation of the Buenos Aires station.

### *3.2. Thunderstorm area*

To analyse the impact of thunderstorm areas on PG, we first conducted a local component analisys based on Yaniv et al. (2016). In this work, daily mean variations of both AOD and temperature on FW days were calculated in order to compare them with the local PG curve (FW).

After, to test the extent to which the daily PG (FW) curve in Buenos Aires Station captures the global thunderstorm signal, the area of thunderstorms was calculated at both global and regional scales. A thunderstorm was defined as any pixel in the global domain of the DiGangi et al. (2021) Thunder Hour Database with a positive detection. To calculate the area, pixel was defined as 0.05° x 0.05° latitude-longitude. The area of each pixel is then calculated and only those pixels that contain an associated thunderstorm are included in the area summation.

In turn, the world has been divided into 4 regions based on the work of Ccopa et al. (2021): Oceania (Oc, 150°E to 120°W), Asia-Australia (AsAus, 60°E to 150°E), Africa-Europe (AfEu, 30°W to 60°E) and America (Am, 120°W to 30°W). Area summation was then performed for each hour of the day at global and regional scales for the complete series of thunder hours. The hourly median was then calculated for the 24 hours of the day for the 5 data series (see Figure 1). Based on these medians, the curves of daily variations of the thunderstorm area medians were constructed for all data series. Daily variations of the quarterly median were also calculated. Finally, the correlations of the daily thunderstorm area median curves of the complete series and of the quarterly scale with the corresponding daily PG (FW) curves were calculated. Fisher's transformation with a confidence interval of 95 % was used to test their significance.

Journal Pre-proof

Figure 1: Map showing the regions used for the thunderstorm area analysis (based on the work of Ccopa et al. (2021)). The red lines demarcate the boundaries of the regions. The regions in question are Oceania (150°E to 120°W), Asia-Australia (60°E to 150°E), Africa-Europe (30°W to 60°E) and the Americas (120°W to 30°W). The red star shows the location of Buenos Aires Station. b) Satellite image of the Buenos Aires station. The red circle indicates where the instruments are installed. c) Photo of the electric field sensor installed at the Buenos Aires station.

# 4. Results

## *4.1. Potential Gradient sample analysis*

The frequency distribution of the hourly mean PG observations evaluated (i.e. 1780 days in the period 2017-2021) is shown in Figure 2.a, using PG values averaged every minute (1440 data per day). In the figure, the vertical axis is constrained to see how the highest frequencies are distributed. Between the two dotted lines corresponding to ± 5 MAD (57.14 $Vm^{-1}$) with respect to the daily median (30.11 $Vm^{-1}$) of the complete series, the highest frequencies of PG occurrences are observed. It can be seen that PG has a higher frequency of occurrence between 0 - 50 $Vm^{-1}$, and as expected PG values have a predominant order of magnitude lower than 100 $Vm^{-1}$ associated with FW. A possible daily wave can be seen, with a clear minimum at around 6 UTC. This is further shown in Figure 3 which shows the distribution of the daily amplitude of the complete PG series and its cumulative frequency. It can be seen that more than 75 % of the days have a daily amplitude less than 400 $Vm^{-1}$ and about 70 % of these data are between 0 $Vm^{-1}$ and 200 $Vm^{-1}$. The remaining 25 % of data with larger amplitudes are distributed over a very wide range and show a large variability.

PG measurements above 5 MAD (approx. 80 $Vm^{-1}$) in Figure 2.a, i.e. above the FW limit, show a relative maximum in the frequency of occurrence at 12 UTC (9 LT) and at 00 UTC (21 LT) of PG values close to 120 $Vm^{-1}$. The frequency of these values is between 1 and 2 orders of magnitude lower than what is observed within the range defined as FW. These PG values could be related to local effects such as pollution resulting from circulation in the highway, but it will not be the focus of this study and requieres further analysis. Additionally, PG values above 120 $Vm^{-1}$

have a very low frequency of occurrence, and are possibly associated with extreme weather events.

The behaviour of PG can differ greatly from one day to the next. Figure 2.b shows this behaviour. Figure 2.b shows the daily mean value for each day of the complete PG series. It clearly shows an annual cycle with peaks in the months of JJA, with some years reaching higher mean values than others. In addition, there are days with mean values that differ from the most frequent ones, such as those with negative or very positive values. These extreme values may possibly be associated with days with storms or precipitating systems.

Figure 2: a) Diurnal variability: Frequency distribution of the hourly mean of PG averaged every minute versus hour (UTC). Colours correspond to the frequency of occurrence in days. The black solid line indicates the daily median of the complete series and the dashed lines correspond to ± 5 MAD (57.14 $Vm^{-1}$). b) Time series: Series of daily average PG values for the complete series (2017-2021). The black solid line indicates the daily median of the complete series.

Figure 3: Frequency histogram of the daily PG amplitude for the complete series (2017-2021) in bars and its normalised cumulative frequency in red. PG values are one-minute averages of samples taken every 5 seconds.

Figure 4 shows the percentage of data belonging to the category FW, DW and missing (na) for each month of the year using the proposed methodology. Each data used is an average per minute of the 12 measurements taken every 5 seconds. Therefore, missing data were defined when more than 25% of the data were missing in that minute. It can be seen that at least 80% of the data are available for each month of the year. There is also an apparent annual cycle in the number of

Journal Pre-proof

FW days. The largest loss of data in August and September is due to a data storage failure. It is clear from Figure 3 that it is not possible to assume that the number of FW days is greater than the number of DW days, as it depends very much on the climatology of the site being analysed, and consequently the importance of establishing methodologies that allow intercomparisons with other measurement sites.

Figure 4: Percentage of amount of PG data considered as good weather (FW), disturbed weather (DW) and no data (NA) for each month of the year.

### *4.2. Analysis of PG in Fair Weather (FW) days and its comparison with the Carnegie Curve*

Applying the methodology described in section 3 to select FW days, 885 days out of 1780 (49.72 %) are obtained that meet the criteria. In order to understand how this series varies on a yearly basis, Figure 5 shows (a) the hourly median PG (FW) for each month of the year in panel and (b) the daily average of the hourly medians. This figure clearly shows a change in the time at which the hourly minimum and maximum occur as the months progress. In the winter months (JJA) the daily maximum occurs later than in the summer months (DJF). On the other hand, the daily minimum shows the same behaviour in both summer and winter, i.e. in JJA the daily minimum occurs at times similar to those of the DJF quarter and earlier in the SON and MAM quarters. As for the monthly mean of the hourly medians, it can be seen in Figure 5.b that in JJA (DJF) the highest (lowest) values occur.

Figure 5.c additionally shows the diurnal variability of the global thunderstorm area over the months of the year in the left panel and the monthly variation of the mean total thunderstorm

area median in the right panel for the whole period 2014 - 2021. This figure shows a daily variation that changes in the time of its extremes depending on the month of the year.

Figure 5: Variability of PG and global thunderstorm areas: a) 2D histogram of hourly median PG (FW) versus time (UTC) and months. Colours correspond to hourly median PG. PG values are one-minute averages of the samples taken every 5 seconds. b) Monthly average of the daily median values. c) 2D histogram of the hourly median of the thunderstorm area ($10^6 km^2$) versus time (UTC) and months. The colours correspond to the hourly median of the thunderstorm area. d) Monthly average of the daily values of the median of the thunderstorm area ($10^6 km^2$).

The daily thunderstorm area maximum reaches its highest values in JJA between 18 and 21 UTC, corresponding to the SH winter. This quarter is also characterized for having the highest PG values too as shown in Figure 5.b. While the minimum thunderstorm area reaches its lowest values in the months of JFD as in PG (FW), although the minimum thunderstorm area is observed between 0 and 3 UTC, about 3 hours earlier than what is observed for PG (see Figure 5.a).

Not all local PG (FW) curves exhibit the same behaviour throughout the day. To illustrate this, Figure 6 presents the local PG (FW) curves as a percentage of their mean value for CITEDEF, Carnegie, Mitzpe-Ramon, and CASLEO. The Mitzpe Ramon curve extracted from Yaniv et al. (2016) was obtained from measurements taken in the Negev Desert (850 meters above sea level) in southern Israel, while the CASLEO curve was derived from observations made at 2480 meters above sea level at the foothills of the Andes in Argentina (Tacza et al., 2021). Figure 6 shows that the observation sites located in Argentina, CITEDEF and CASLEO, exhibit a single maximum after 15 UTC. In contrast, the site in Israel has two peaks: the first around 11 UTC and the second

around 21 UTC. Regarding the time of the minimum value, there is a coincidence in the Mitzpe Ramon and CASLEO curves where the minimum occurs at around 4 UTC. On the other hand, CITEDEF reaches its absolute minimum around 6 UTC, two hours later than the aforementioned stations. Finally, its similarity with the variation shown in 2 can be highlighted, with a minimum at hours close to 6 UTC and higher values at later hours.

Figure 6: PG (FW) curves as a percentage of their mean value for: CITEDEF in blue dashed line and its standard deviation in pink shading, Carnegie curve (from Harrison (2004)) in red solid line, CASLEO in green dotted line (data supplied by Dr. Jose Tarza) and Mitzpe Ramon in magenta dashdot line (from Yaniv et al. (2016)). The lower horizontal axis shows the time in UTC hours while the upper horizontal axis shows the time in local time (LT). The values in the legends correspond to daily averages in FW days.

The amplitude peak to peak of the local curve shows a value close to 30% (15 $Vm^{-1}$) of that corresponding to the Carnegie Curve (45 $Vm^{-1}$). The mean values do not match either, with the local value having a mean of 30 $Vm^{-1}$ and the Carnegie value having a value close to 130 $Vm^{-1}$. The maxima and minima also show a different hourly distribution. The Carnegie minimum is reached at 3 UTC, while the maximum is reached around 19 UTC, the latter associated with electrical activity in the Americas, Africa and Europe (there is another peak at 8 UTC associated with activity in Asia-Australia) as shown in previous studies. Locally, the PG minimum is reached at 6 UTC and a maximum peak is reached at 16 UTC. There is also a positive correlation with a confidence level of 95 % and the value of the Spearman correlation coefficient (R) between the two curves is 0.83.

Journal Pre-proof

Analyzing the annual daily mean local PG (FW) curve behaviour, Figure 7.a shows that the last 5 years show a similar behaviour in terms of their shape. A difference in their mean values can be observed however. Special attention is given to 2020 which has the lowest values, while 2019 seems to have the highest values. Figure 7.b shows the annual box plots of the daily medians calculated for the FW days. A variation of the median (black line) can be seen over the years. The dispersion of the data is also different, especially when comparing 2019 and 2021.

Figure 7: Annual variability in the daily PG (FW) curve at Buenos Aires Station: a) Daily mean PG (FW) curves ($Vm^{-1}$, 2017-2021) by years in colours. These curves are derived from the PG(FW) series. b) Boxplot for FW days: daily median PG (FW) ($Vm^{-1}$) for all years analysed (2017-2021). Plus signs indicate outliers

In order to assess the local and global effects on the measured curve, the local PG (FW) curve in CITEDEF was compared to the average behaviour of temperature and AOD at the 440 nm channel for the FW days (885 days between 2017 and 2021) in Figure 8. The results differ from what was presented in Yamv et al. (2016), as there is a clear phase shift between the temperature curve and the PG curve; the local PG (FW) curve starts to rise from 6 UTC, while the temperature curve does so after 9 UTC. As for AOD, it appears to follow the temperature behaviour but not that of PG (FW). This supports the idea that the local aerosol-related effect and the sunrise effect are not the dominant factors affecting the local PG (FW) curve.

Figure 8: Daily PG (FW) curve in light blue dashed line (left vertical axis), daily mean temperature curve in FW days in purple dash-dotted line (main right vertical axis) and daily average AOD

variation on FW days in green dotted line

(secondary right vertical axis). The lower horizontal axis shows the time in UTC hours while the upper horizontal axis shows the time in universal time (UTC).

Therefore, once a simple evaluation of the local effects has been conducted, we proceed to compare the local PG (FW) curve with the global thunderstorm area. In order to do this, we analyze the diurnal variation of the calculated global hourly median thunderstorm area in Figure 9 (represented by the light blue dashed line) on the right axis and for different regions on the left axis. It can be seen that the regional maxima occurs later in the day the further west the region is from 150° E, except for the Oceania region. This oceanic region reaches its maximum 1 hour before the time of the African/Asian maximum. The maximum of the Asian/Australian region occurs around 8 UTC, that of the African/European region around 15 UTC, that of Oceania around 14 UTC, and finally that of the American region between 19 and 20 UTC. The shift in the time of maximum is consistent with the longitudinal position of the continents and the radiative cycle in each region, as the highest temperatures in UTC time are reached later the further west the region is located. From the global curve, it can be seen that the minimum median thunderstorm area occurs at 3 UTC and the maximum around 19:30 UTC, and that it is very similar to the Carnegie Curve Harrison (2004) and the local PG (FW) curve (R = 0.83).

Figure 9: Diurnal variation of the global median thunderstorm area (light blue) associated with the right vertical axis and separated by regions on the left vertical axis. The regions used are the Americas (burgundy), Africa and Europe (red), Asia and Australia (green) and Oceania (violet). The period used for this calculation was 2014-2021.

Journal Pre-proof

To quantify the correlation between the daily PG curve (FW) at Buenos Aires Station and the hourly median variation of the thunderstorm area we use the Spearman correlation coefficient. Not only at the global scale (Tot on the far left), but also at the regional scale for the regions of interest (i.e. America, Africa and Europe, Asia and Australia, and Oceania), and for possible combinations of these regions. These correlations are shown in Figure 10. Only significant correlations are discussed below, discarding those that are not significant (boxes shown with white diagonal lines fill patterns). The correlation between the daily PG curve (FW) and the daily median of the global thunderstorm area (Tot) has an R value of 0.83. Therefore, the value of $R^2$ is 0.689, which means that 68.9 % of the daily PG (FW) curve can be explained by the global scale thunderstorm area. When combining three regions, the maximum correlation value is reached by combining the regions of America, Europe, Africa and Oceania (Am-AfEu-oc) with an r value of 0.90 (i.e., $R^2$ value implying 81.0 % of the daily PG (FW) curve can be explained by the sum of the thunderstorm areas of these three regions. The minimum is reached by combining Asia, Australia, Africa, Europe and Oceania (AsAus-AfEu-oc) with an R-value of 0.67. When combining two regions, the maximum correlation is reached by combining Africa, Europe and Oceania (AfEu-oc) with a value of 0.93, so the value of $R^2$ implies that 87.0% of the daily PG curve (FW) can be explained by the thunderstorm area of these regions. The minimum is reached by combining Africa, Europe, Asia and Australia (AfEu-AsAus) with an R value of 0.69. When analysed by region, the highest correlation is found for the Africa-Europe region (AfEu) with an R value of 0.95, indicating that 90.3 % of the daily PG curve (FW) can be explained by the thunderstorm area of Africa and Europe. The high correlations of both the global scale area and the combined or individual regions show that the large scale effect explains more of the daily PG (FW)

curve than could be explained by the weather phenomena occurring over the Buenos Aires Station. It can also be seen that when combining regions, Asia and Australia (AsAus) contribute to a decrease in the correlation values, while Africa and Europe (AfEu) increase them due to the time of occurrence of maxima and minima in Africa-Europe with respect to the daily PG (FW) curve. The three highest R values (greater than or equal to 0.9) include the AfEu region.

Figure 10: Heat map of Spearman correlation coefficients between the PG (FW) curve ($Vm^{-1}$) calculated for the period 2017-2021 and the different combinations of regions, including the global thunderstorm area, in the period 2014-2021. Boxes with a white diagonal line pattern indicate a lack of significant correlation. Am refers to the Americas, AfEu to Africa and Europe, AsAus to Asia and Australia, Oceania to Oceania, and Tot to the sum of all regions. Tests were performed at a significance level of 0.05.

The next step is to analyze the seasonal variations of these correlations. Figure 11 shows the diurnal variation of thunderstorm area and the local mean PG (FW) curve for the 4 quarters of the year (DJF, MAM, JJA, SON). The southern hemisphere seasons will be used in the following discussion. A similar behaviour in the two curves can be observed in the spring (SON) and autumn (MAM) quarters (see Figure 11.b and Figure 11.d), with PG (FW) minimum values close to 20 $Vm^{-1}$ and maximum values close to 37 $Vm^{-1}$. On the other hand, the summer quarter (DJF, see Figure 11.a) has lower values than the above quarters. The winter quarter (JJA, see Figure 11.c), on the other hand, is the one with a daily mean curve with values that always exceed the other three quarters and it has a very different behaviour for the late afternoon/night hours. The minimum PG for all quarters is observed between 6 UTC and 7:30 UTC, with the JJA quarter reaching the

earliest minimum and the DJF quarter at the latest. The maximum PG values for the autumn and spring quarter are observed between 12 and 21 UTC. The summer quarter reaches its maximum PG values a little earlier, between 14 and 17 UTC. Finally, the winter quarter reaches its maximum PG value of around 22 UTC. This quarter is the only one to reach its maximum PG values after 20 UTC.

Figure 11: Daily PG (FW) curves (dashed lines) and Daily variations of the global median thunderstorm area (solid lines) by quarters: a) December-January-February (DEF), b) March-April-May (MAM), c) June-July-August (JJA) and d) September-October-November (SON). Daily PG (FW) curves are derived from the FW-EF series. Daily variations of the global median thunderstorm area have been calculated for the period 2014-2021.

To quantify the relationship between the global thunderstorm area and the mean PG (FW) curve, Figure 12 is shown. The Figure shows the Spearman's correlation coefficient between PG at the quarterly scale and the daily variations of the median total thunderstorm area for each quarter of the year (summer: DJF, autumn: MAM, winter: JJA and spring: SON) at global, regional and different combinations of the 4 study regions. Figure 11.c shows the highest values of both thunderstorm areas and PG(FW) in the JJA - the winter (summer) quarter of the southern (northern) hemisphere. The lowest values are reached in the DJF (see Figure 11.a), winter (summer) quarter of the southern (northern) hemisphere. Southern hemisphere spring (SON) exceeds southern hemisphere autumn thunderstorm area values. An analysis of the correlation values in Figure 12 shows a good positive correlation between the quarterly PG curves and the global thunderstorm area curves (Tot), with a maximum correlation in summer and spring (R=

0.81) and a minimum in winter (R= 0.79). As in Figure 10, values with a line indicate the absence of a significant correlation ($p < 0.05$).

The daily variations of the median thunderstorm area in all quarters show 2 maxima, one absolute and one relative (see Figure 11). The absolute maximum corresponds to the time at which the maximum thunderstorm area occurs in the American region after 15 UTC, except in the MAM quarter (see Figure 11.b). The relative maximum, except in the MAM quarter which represents the absolute maximum, corresponds to the time when the maximum thunderstorm area occurs in Africa and Europe (between 12 and 15 UTC). In the summer (DJF) and spring (SON) quarters(see Figure 11.a and Figure 11.d respectively), there is a second relative maximum, in this case associated with the rest of the continental region, Asia and Australia, which occurs before 8 UTC. When analysing the maxima of the daily PG (FW) curves, it can be observed that the JJA quarter has the absolute maximum around 22 UTC, which coincides with the absolute maximum of the daily variation of the median thunderstorm area of the same quarter. The other quarters have their maximum between 15 and 17 UTC.

It can be seen that the total thunderstorm area does not have the highest correlation with the PG (FW) compared to other regional combinations in Figure 12. In the breakdown of the regional thunderstorm areas and possible combinations, it can be seen that when three regions are combined, the combination of America, Africa, Europe and Oceania (Am-AfEu-oc) (see Figure 10) are again the combination that reach the highest R values in most quarters (except for SON when it is AfEu and AfEu-oc). The highest correlation is obtained in the MAM quarter (R=0.96). When combining two regions it is not the same as in Figure 10, the highest correlations are generally obtained when combining America, Africa and Europe (Am-AfEu). The maximum value of R is reached in the MAM quarter and the minimum in SON. For DJF, when PG (FW)

Journal Pre-proof

mainly shows the lowest seasonal values, the maximum correlation is with Africa, Europe and Oceania (AfEu-Oc), while for the quarter in which the maximum of the daily PG (FW) curve occurs, JJA, the maximum correlation is with America, Africa and Europe (Am-AfEu). As for the correlation values of the regions at the individual level, the Africa and Europe region is the only one with significant values in all 4 quarters. This region also has the highest correlation values when compared with the significant correlations of the other regions.

Figure 12: Heat map of Spearman correlation coefficients between PG($Vm^{-1}$) at the quarterly level in the period 2017-2021 and the combination of regions and global thunderstorm area at the quarterly level. Values with a line indicate a lack of significant correlation. Am refers to the Americas region, AfEu to Africa and Europe, AsAus to Asia and Australia, Oceania to Oceania and Tot to the sum of all regions. Tests were performed at a 0.05 level of significance.

## 5. Conclusions

In order to make future comparisons, this paper proposes to use a methodology for selecting FW days that does not require meteorological data and/or elimination of days with arbitrary thresholds. For this purpose, the definition of deviation proposed by Lucas et al. (2017) and the median are used to define a methodology that identifies FW days. By applying this method in the analysis of PG variability (FW) at Buenos Aires Station, it was possible to distinguish a daily variation throughout the year that reaches a maximum in the winter months (JJA) and a minimum in the summer months (DJF), as previously reported by Tacza et al. (2018) for San Juan. There is also a shift in the time of both the daily maximum and minimum as the year progresses. As for the annual variation, it has an amplitude of about 10 $Vm^{-1}$, which is similar to the order of magnitude

observed in Lucas et al. (2017).

The results show that the daily PG (FW) curve has a good correlation with the Carnegie curve (R=0.83). This result is expected, since in Velazquez (2021) a good correspondence had already been found in Buenos Aires Station between the Carnegie Curve and the daily mean PG (FW) curves using two different FW methodologies, one statistical and the other meteorological. Similarly, Tacza et al. (2018) had found a correlation of 0.94 for San Juan. The good correlation shows that the methodology chosen in this work successfully selects FW days that detect the GEC signal, which is desirable for future studies.

In the analysis between AOD, temperature and PG, it was observed that the local effects do not have a predominant effect on the PG (FW) daily curve. On this basis, we proceeded to study the global thunderstorm effect from the GEC on the PG (FW) curve. Thunder hour data from DiGangi et al. (2021) was used to calculate the thunderstorm area and verify whether the local daily mean PG (FW) curve was capturing the global thunderstorm signal. The global thunderstorm area showed a similar monthly behaviour to that of the PG (FW) series. Similarly to PG (FW) values, maximum thunderstorm areas were observed in the JJA quarter and minimum areas were observed in the DJF quarter as previously shown in the work of Adlerman and Williams (1996). This is explained by a larger continental area in the NH than in the HS (Mezuman et al., 2014). Regarding the monthly pattern with respect to the time of the day, a great similarity is observed both in the PG (FW) field and in the thunderstorm areas, indicating a good correspondence between the two variables. The correlation between the local PG (FW) curve and, both the total thunderstorm area and the area for different regions of interest (i.e., Oc., AsAus., AfEum and America) and their possible combinations was analysed. The local mean PG (FW) curve is highly correlated to the total thunderstorm area (R=0.83), Am-Af-Eu (R=0.88) and Af-Eu (R=0.93). This

indicates that the global thunderstorm signal is captured well by the local daily PG (FW) curve at Buenos Aires Station. Similar correlations were found in the seasonal analysis.

The daily median global thunderstorm area curve shows 3 maxima associated with the 3 regions with the largest land masses, the Americas, Africa/Europe and Asia/Australia. The calculated positions of the maximum and minimum associated with each region correspond to those previously show by calculated by Peterson et al. (2018). Similarly, Blakeslee et al. (2014) using flash per seconds, a very different approach, reached a similar conclusion. This is important because it shows that the calculated thunderstorm area is a good proxy to represent the GEC and its correlation with the local curve.

The results obtained show that the methodology used in this work is robust and it can be used in the absence of meteorological data. This methodology will be the basis for future work, as its performance has shown that it is able to preserve the large-scale thunderstorm area signal and therefore the GEC signal. The results presented suggest that the aerosol effect, the sunrise effect, and/or their combination may not be the dominant factors influencing the behaviour of the local PG (FW) curve. However, future work will specifically analyse the impact of pollution, industrial activities, construction sites, and natural dust sources on local PG (FW) measurements in Buenos Aires.

Journal Pre-proof

## Data availability

The datasets are freely available to the scientific community in the CONICET repository: `http://hdl.handle.net/11336/217041`.

## Acknowledgements

Thunder hour data was provided by Earth Networks, in collaboration with WWLLN (available at http://thunderhours.earthnetworks.com). The CASLEO PG (FW) curve was provided by Dr. José Tacza. This research was supported by the Ministry of Defense through MINDEF PIDDEF 07/18: Environmental Risk Information Platform; and GeoRayos II and CITEDEF with the GeoRayos II WEB Project and GINKGO 03 NAC 040/1. Yasmin Velazquez is supported by the National Scientific and Technical Research Council (CONICET). Finally, the authors gratefully acknowledge the GLOCAEM project partners (listed at https://glocaem.wordpress.com/introduction/project-partners-and-measurement-sites) and the Natural Environment Research Council (NERC) grant NE/N013689/1 for the provision of the GLOCAEM data.

## References

Adlerman, E.J., Williams, E.R., 1996. Seasonal variation of the global electrical circuit. Journal of Geophysical Research: Atmospheres 101, 29679–29688. doi:https://doi.org/10.1029/96JD01547.

Afreen, S., Victor, N.J., Nazir, S., Siingh, D., Bashir, G., Ahmad, N., Javid Ahmad, S., Singh, R., 2022. Fair-weather atmospheric electric field measurements at gulmarg, india. Journal of Earth System Science 131, 1–19. doi:https://doi.org/10.1007/s12040-021-01745-5.

Journal Pre-proof

Anisimov, S.V., Galichenko, S.V., Aphinogenov, K.V., Prokhorchuk, A.A., 2018. Evaluation of the atmospheric boundary-layer electrical variability. Boundary-Layer Meteorology 167, 327–348. doi:https://doi.org/10.1007/s10546-017-0328-0.

Blakeslee, R.J., Mach, D.M., Bateman, M.G., Bailey, J.C., 2014. Seasonal variations in the lightning diurnal cycle and implications for the global electric circuit. Atmospheric research 135, 228–243. doi:https://doi.org/10.1016/j.atmosres.2012.09.023.

Bogo, H., Negri, R.M., San Rom/an, E., 1999. Continuous measurement of gaseous pollutants in buenos aires city. Atmospheric Environment 33, 2587–2598. doi:https://doi.org/10.1016/S1352-2310(98)00270-2.

Buzás, Attila, A, N.K., André, S., Karolina, Bór, J., 2022. Comparison of different atmospheric electric fair weather criteria based on potential gradient data.

Buzás, A., Barta, V., Horváth, T., Bór, J., 2021. Revisiting the long-term decreasing trend of atmospheric electric potential gradient measured at nagycenk, hungary, central europe, in: Annales Geophysicae, Copernicus GmbH. pp. 627–640. doi:https://doi.org/10.5194/angeo-39-627-2021.

Canton, J., 1753. Liii. electrical experiments, with an attempt to account for their several phænomena; together with some observations on thunderclouds. Philosophical Transactions of the Royal Society of London, 350–358 doi:https://doi.org/10.1098/rstl.1753.0053.

Ccopa, J.A., Tacza, J., Raulin, J.P., Morales, C.A., 2021. Estimation of thunderstorms occurrence from lightning cluster recorded by wwlln and its comparison with the ‘universal’carnegie

curve. Journal of Atmospheric and Solar-Terrestrial Physics 221, 105682. doi:https://doi.org/10.1016/j.jastp.2021.105682.

DiGangi, E.A., Stock, M., Lapierre, J., 2021. Thunder hours: How old methods offer new insights into thunderstorm climatology. Bulletin of the American Meteorological Society, 1–47 doi:https://doi.org/10.1175/BAMS-D-20-0198.1.

Frank-Kamenetsky, A., Burns, G., Troshichev, O., Papitashvili, V., Bering, E., French, W., 1999. The geoelectric field at vostok, antarctica: its relation to the interplanetary magnetic field and the cross polar cap potential difference. Journal of Atmospheric and Solar-Terrestrial Physics 61, 1347–1356. doi:https://doi.org/10.1016/S1364-6826(99)00089-9.

Gurmani, S., Ahmad, N., Tacza, J., Iqbal, T., 2018. First seasonal and annual variations of atmospheric electric field at a subtropical station in islamabad, pakistan. Journal of Atmospheric and Solar-Terrestrial Physics 179, 441–449. doi:https://doi.org/10.1016/j.jastp.2018.09.011.

Harrison, R., Nicoll, K., 2018. Fair weather criteria for atmospheric electricity measurements. Journal of Atmospheric and Solar-Terrestrial Physics 179, 239–250. doi:https://doi.org/10.1016/j.jastp.2018.07.008.

Harrison, R.G., 2004. The global atmospheric electrical circuit and climate. Surveys in Geophysics 25, 441–484. doi:https://doi.org/10.1007/s10712-004-5439-8.

INDEC, 2022. Censo nacional de poblacion, hogares y viviendas 2022. Censo 2022: Resultados Provisionales, Instituto Nacional de Estadıstica y Censos. Buenos Aires, Argentina, in Spanish.

Journal Pre-proof

Israel, H., 1973. Atmospheric electricity, vol. ii. Israel program for scientific translations, Jerusalem (trans. from German).

Kamogawa, M., Suzuki, Y., Sakai, R., Fujiwara, H., Torii, T., Kakinami, Y., Watanabe, Y., Sato, R., Hashimoto, S., Okochi, H., et al., 2015. Diurnal variation of atmospheric electric field at the summit of mount fuji, japan, distinctly different from the carnegie curve in the summertime. Geophysical Research Letters 42, 3019–3023. doi:https://doi.org/10.1002/2015GL063677.

Kumar, S., Siingh, D., Singh, R., Singh, A., Kamra, A., 2018. Lightning discharges, cosmic rays and climate. Surveys in Geophysics 39, 861–899. doi:https://doi.org/10.1007/s10712-018-9469-z.

Lapierre, J., Stock, M., DiGangi, E., 2021. Lightning detection network performance for thunderstorms, in: 101st American Meteorological Society Annual Meeting, AMS.

Liu, C., Williams, E.R., Zipser, E.J., Burns, G., 2010. Diurnal variations of global thunderstorms and electrified shower clouds and their contribution to the global electrical circuit. Journal of the atmospheric sciences 67, 309–323. doi:https://doi.org/10.1175/2009JAS3248.1.

Lucas, G.M., Thayer, J.P., Deierling, W., 2017. Statistical analysis of spatial and temporal variations in atmospheric electric fields from a regional array of field mills. Journal of Geophysical Research: Atmospheres 122, 1158–1174. doi:https://doi.org/10.1002/2016JD025944.

Mach, D.M., Blakeslee, R.J., Bateman, M.G., 2011. Global electric circuit implications of combined aircraft storm electric current measurements and satellite-based diurnal

lightning statistics. Journal of Geophysical Research: Atmospheres 116. doi:https://doi.org/10.1029/2010JD014462.

Mezuman, K., Price, C., Galanti, E., 2014. On the spatial and temporal distribution of global thunderstorm cells. Environmental Research Letters 9, 124023.

Nicoll, K.A., Harrison, R.G., Barta, V., Bor, J., Brugge, R., Chillingarian, A., Chum, J., Georgoulias, A., Guha, A., Kourtidis, K., et al., 2019. A global atmospheric electricity monitoring network for climate and geophysical research. Journal of Atmospheric and Solar-Terrestrial Physics 184, 18–29. doi:https://doi.org/10.1016/j.jastp.2019.01.003.

Peterson, M., Deierling, W., Liu, C., Mach, D., Kalb, C., 2018. A trmm assessment of the composition of the generator current that supplies the global electric circuit. Journal of Geophysical Research: Atmospheres 123, 8208–8220. doi:https://doi.org/10.1029/2018JD028844.

Rycroft, M., Israelsson, S., Price, C., 2000. The global atmospheric electric circuit, solar activity and climate change. Journal of Atmospheric and Solar-Terrestrial Physics 62, 1563–1576. doi:https://doi.org/10.1016/S1364-6826(00)00112-7.

Rycroft, M.J., Harrison, R.G., Nicoll, K.A., Mareev, E.A., 2008. An overview of earth's global electric circuit and atmospheric conductivity. Planetary Atmospheric Electricity, 83–105doi:https://doi.org/10.1007/s11214-008-9368-6.

Sverdrup, H.U., 1944. Scientific results of cruise vii of the carnegie during 1928-1929 under command of captain jp ault: oceanography. .

Tacza, J., Raulin, J., Marun, A., Fernandez, G., 2018. On the variation of the atmospheric electric field in south america: The afinsa network.

Journal Pre-proof

Tacza, J., Raulin, J.P., Macotela, E., Marun, A., Fernandez, G., Bertoni, F.C.P., Lima, L.M., Samanes, J., Buleje, Y., Correia, E., et al., 2020. Local and global effects on the diurnal variation of the atmospheric electric field in south america by comparison with the carnegie curve. Atmospheric Research 240, 104938. doi:https://doi.org/10.1016/j.atmosres.2020.104938.

Tacza, J., Raulin, J.P., Morales, C., Macotela, E., Marun, A., Fernandez, G., 2021. Analysis of long-term potential gradient variations measured in the argentinian andes. Atmospheric Research 248, 105200. doi:https://doi.org/10.1016/j.atmosres.2020.105200.

Velazquez, Y.R., 2021. Estudio del Gradiente de Potencial (Campo Eléctrico Vertical) Atmosf/erico en la zona de Villa Martelli, sus implicancias locales y globales. Master's thesis. Universidad de Buenos Aires. doi:http://dx.doi.org/10.13140/RG.2.2.31549.23522.

Victor, N.J., Chandra, S., Siingh, D., 2020. Lightning, the global electric circuit, and climate. Techniques for Disaster Risk Management and Mitigation, 93–109doi:https://doi.org/10.1002/9781119359203.ch8.

Whipple, F., 1929. On the association of the diurnal variation of electric potential gradient in fine weather with the distribution of thunderstorms over the globe. Quarterly Journal of the Royal Meteorological Society 55, 1–18. doi:https://doi.org/10.1002/qj.49705522902.

Williams, E., Mareev, E., 2014. Recent progress on the global electrical circuit. Atmospheric Research 135, 208–227. doi:https://doi.org/10.1016/j.atmosres.2013.05.015.

Journal Pre-proof

Williams, E., Markson, R., Heckman, S., 2005. Shielding effects of trees on the measurement of the earth's electric field: Implications for secular variations of the global electrical circuit. Geophysical research letters 32. doi:https://doi.org/10.1029/2005GL023717.

Yaniv, R., Yair, Y., Price, C., Katz, S., 2016. Local and global impacts on the fair-weather electric field in israel. Atmospheric Research 172, 119–125.

Yaniv, R., Yair, Y., Price, C., Mkrtchyan, H., Lynn, B., Reymers, A., 2017. Ground-based measurements of the vertical e-field in mountainous regions and the "austausch" effect. Atmospheric Research 189, 127–133. doi:https://doi.org/10.1016/j.atmosres.2017.01.018.

Journal Pre-proof

Journal Pre-proof

Yasmin R. Velazquez: Conceptualization, Methodology, Software, Validation, Formal analysis, Investigation, Writing - Review & Editing, Visualization, Writing - Original Draft.
M. Gabriela Nicora: Conceptualization, Methodology, Investigation, Writing - Original Draft, Writing - Review & Editing, Supervision, Resources.
Vito S. Galligani: Conceptualization, Methodology, Investigation, Writing - Review & Editing, Supervision, Writing - Original Draft.
E. A. Wolfram: Writing - Review & Editing, Supervision.
P. V. Salio: Writing - Review & Editing, Supervision, Data Curation.
Raul L. D'Elia: Data Curation, Writing - Review & Editing.

Journal Pre-proof

**Declaration of interests**

☒The authors declare that they have no known competing financial interests or personal relationships that could have appeared to influence the work reported in this paper.

☐The authors declare the following financial interests/personal relationships which may be considered as potential competing interests:

Journal Pre-proof

- The daily PG curve (FW) in Buenos Aires has a correlation of 0.83 with the Carnegie curve with 95% confidence.
- The daily PG (FW) curve in Buenos Aires has a seasonal variation that accompanies the global changes of thunderstorm areas.
- Local effects such as pollution from a near highway are not dominating the PG (FW) curve behaviour.

Journal Pre-proof

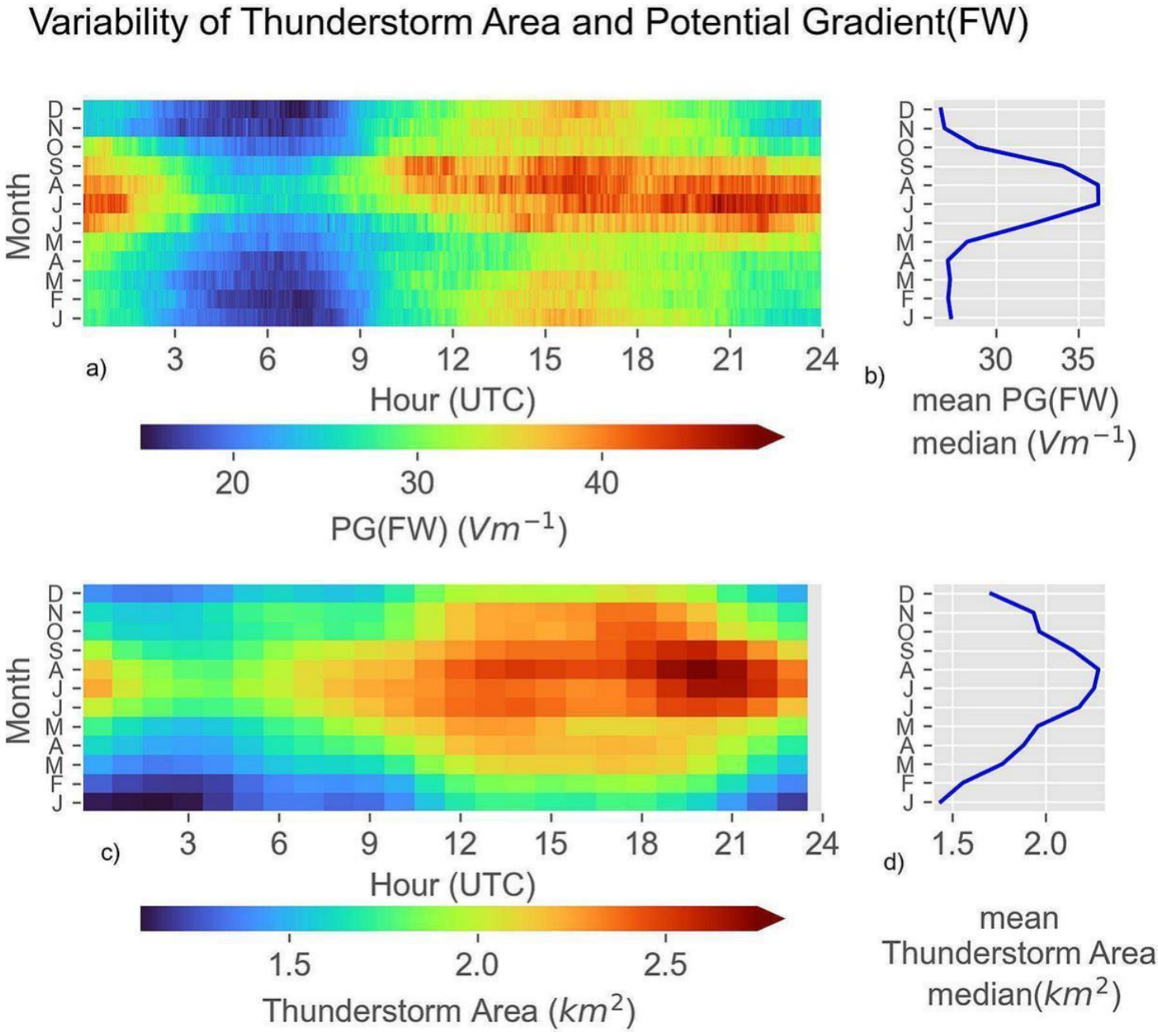


Graphics Abstract

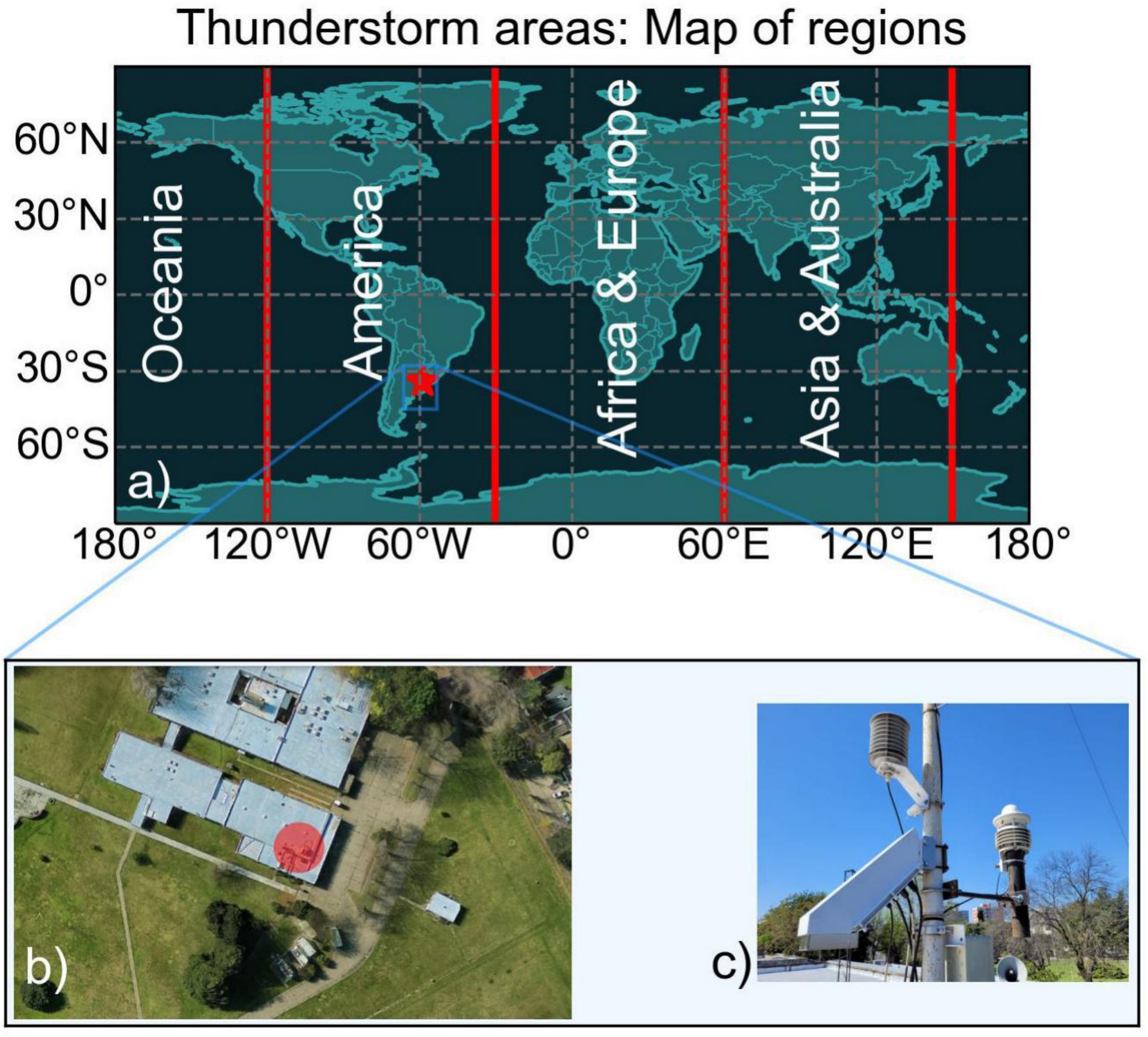
Thunderstorm areas: Map of regions
60°N
30°N
0°
30°S
60°S
Oceania
America
Africa & Europe
Asia & Australia
a)
180°
120°W
60°W
0°
60°E
120°E
180°
b)
c)

Figure 1

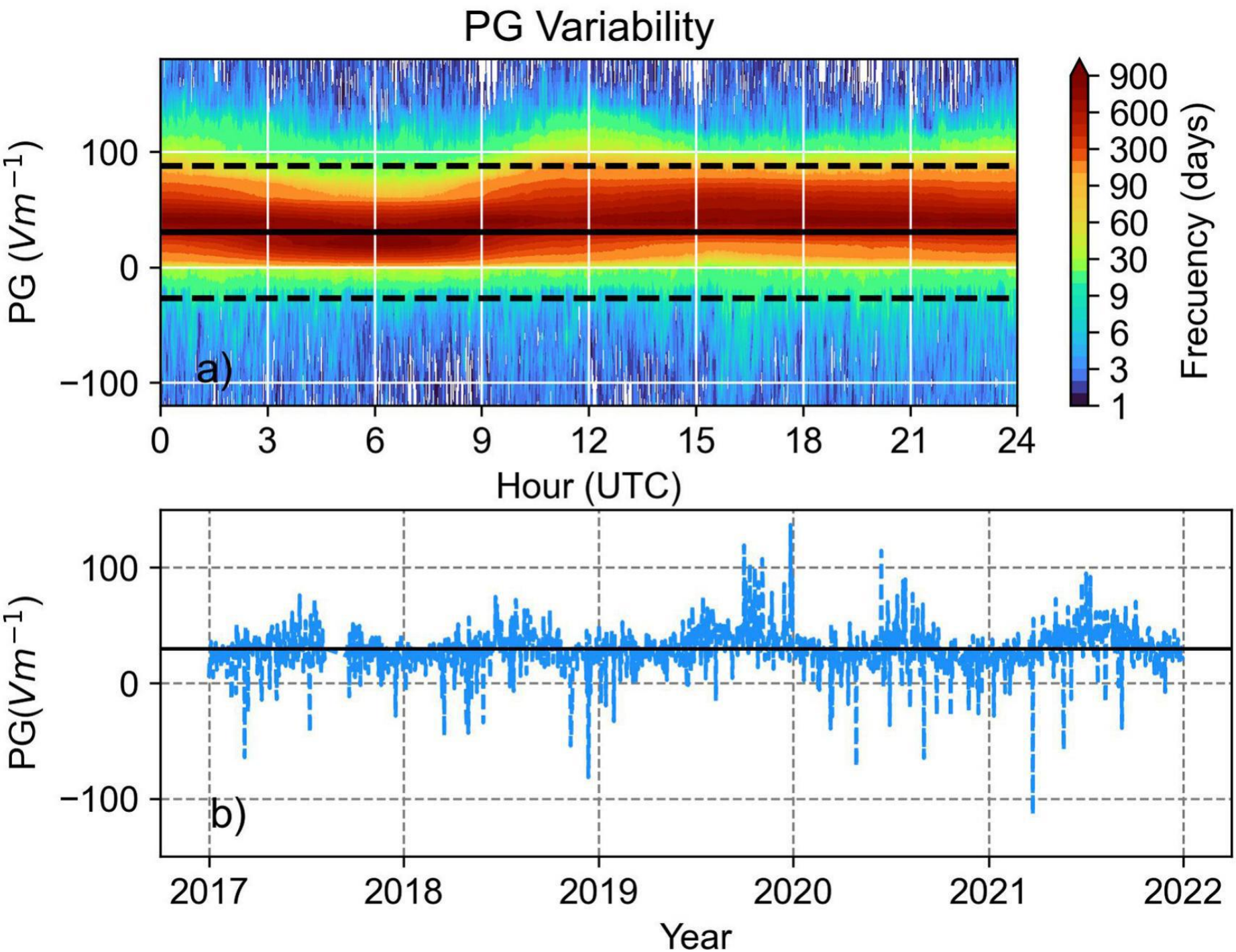
PG Variability
PG (Vm⁻¹)
100
0
−100
a)
0
3
6
9
12
15
18
21
24
Hour (UTC)
900
600
300
90
60
30
9
6
3
1
Frecuency (days)
PG(Vm⁻¹)
100
0
−100
b)
2017
2018
2019
2020
2021
2022
Year

Figure 2

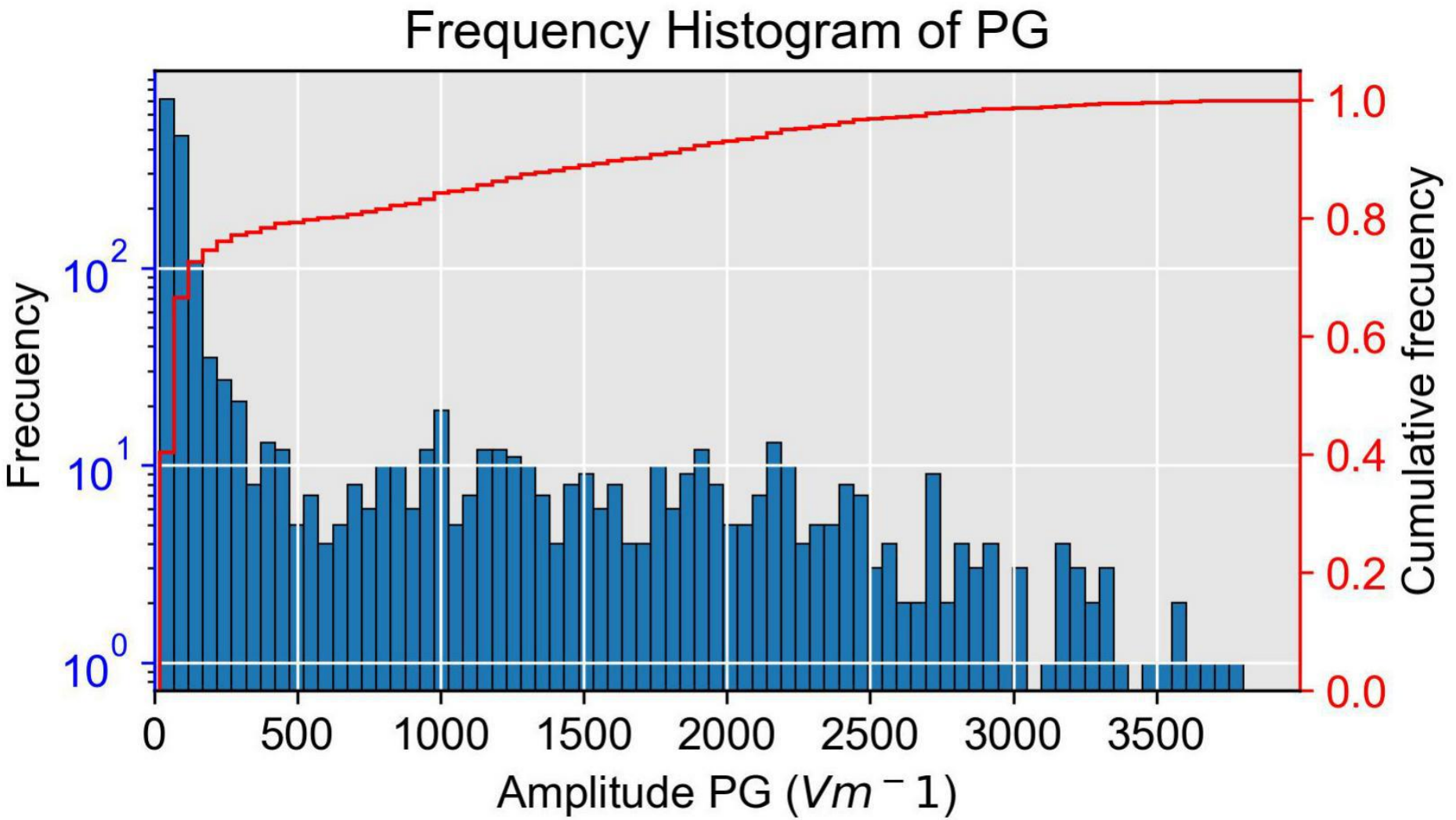
Frequency Histogram of PG
Frecuency
$10^2$
$10^1$
$10^0$
1.0
0.8
0.6
0.4
0.2
0.0
Cumulative frecuency
0
500
1000
1500
2000
2500
3000
3500
Amplitude PG ($Vm^-1$)

Figure 3

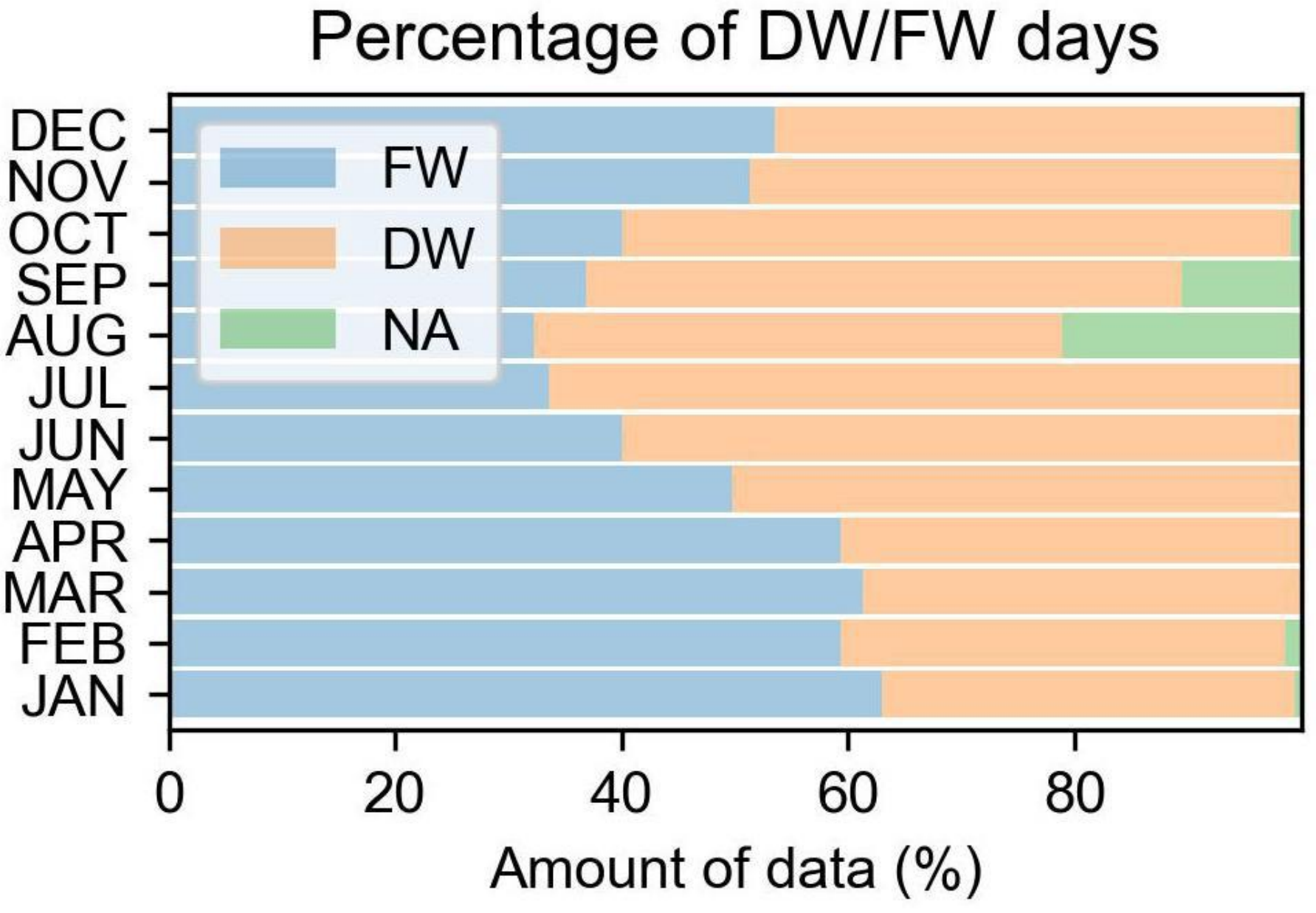
Percentage of DW/FW days
DEC
NOV
OCT
SEP
AUG
JUL
JUN
MAY
APR
MAR
FEB
JAN
FW
DW
NA
0
20
40
60
80
Amount of data (%)

Figure 4

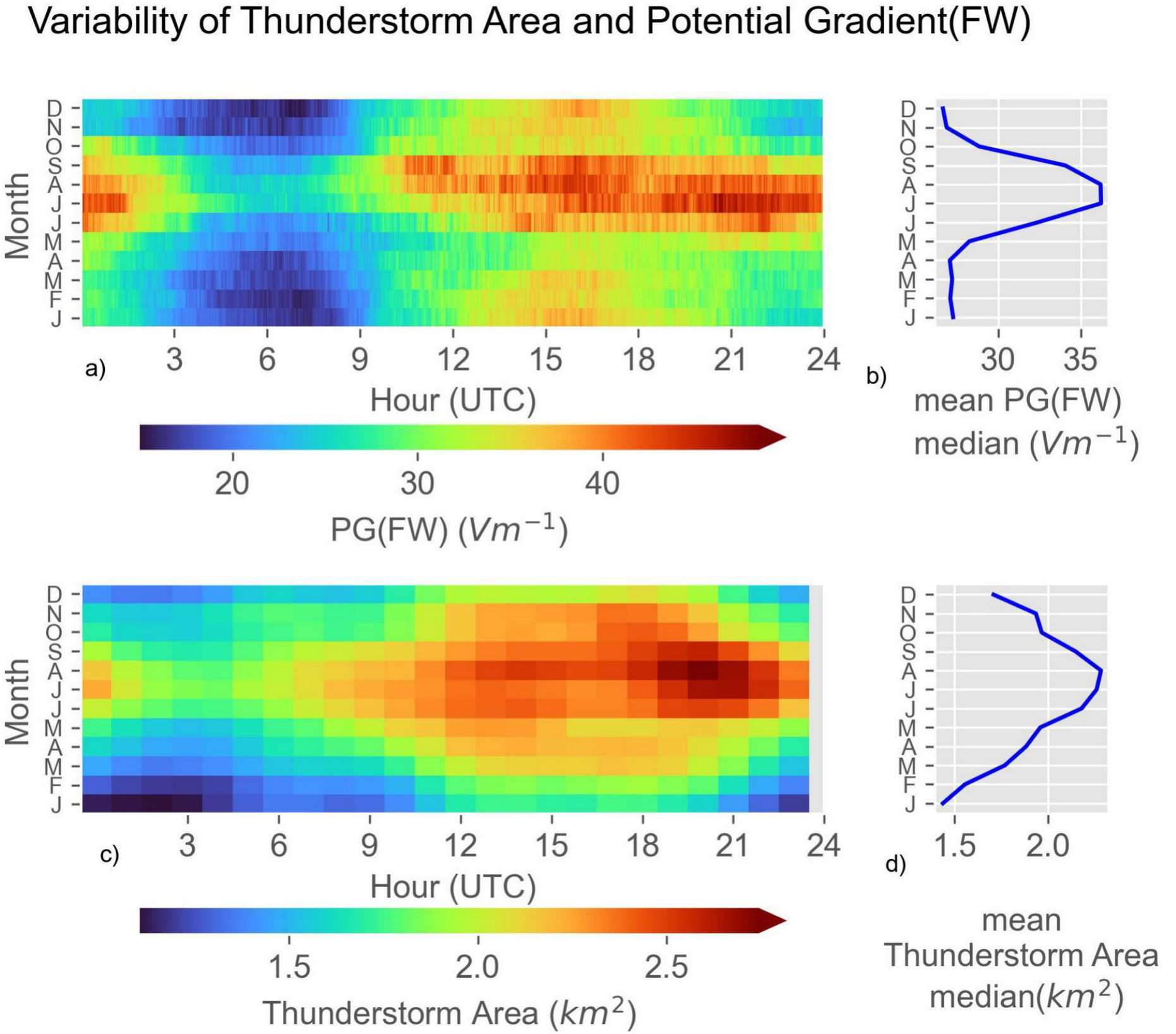
Variability of Thunderstorm Area and Potential Gradient(FW)
Month
D
N
O
S
A
J
J
M
A
M
F
J
3
6
9
12
15
18
21
24
a)
Hour (UTC)
20
30
40
PG(FW) ($Vm^{-1}$)
b)
30
35
mean PG(FW)
median ($Vm^{-1}$)
c)
Hour (UTC)
1.5
2.0
2.5
Thunderstorm Area ($km^2$)
d)
1.5
2.0
mean
Thunderstorm Area
median($km^2$)

Figure 5

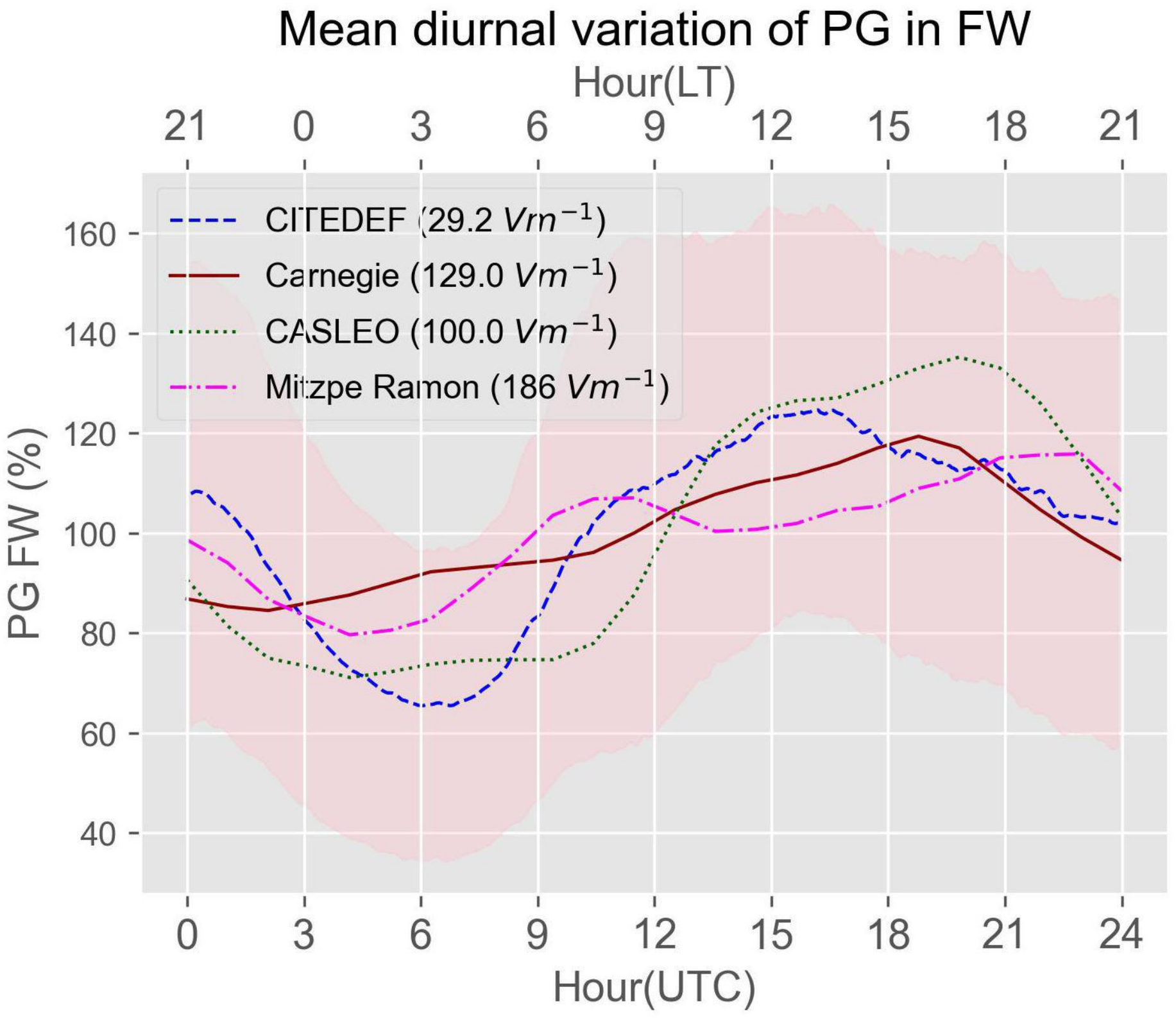
Mean diurnal variation of PG in FW
Hour(LT)
21
0
3
6
9
12
15
18
21
CITEDEF (29.2 $Vm^{-1}$)
Carnegie (129.0 $Vm^{-1}$)
CASLEO (100.0 $Vm^{-1}$)
Mitzpe Ramon (186 $Vm^{-1}$)
160
140
120
100
80
60
40
PG FW (%)
0
3
6
9
12
15
18
21
24
Hour(UTC)

Figure 6

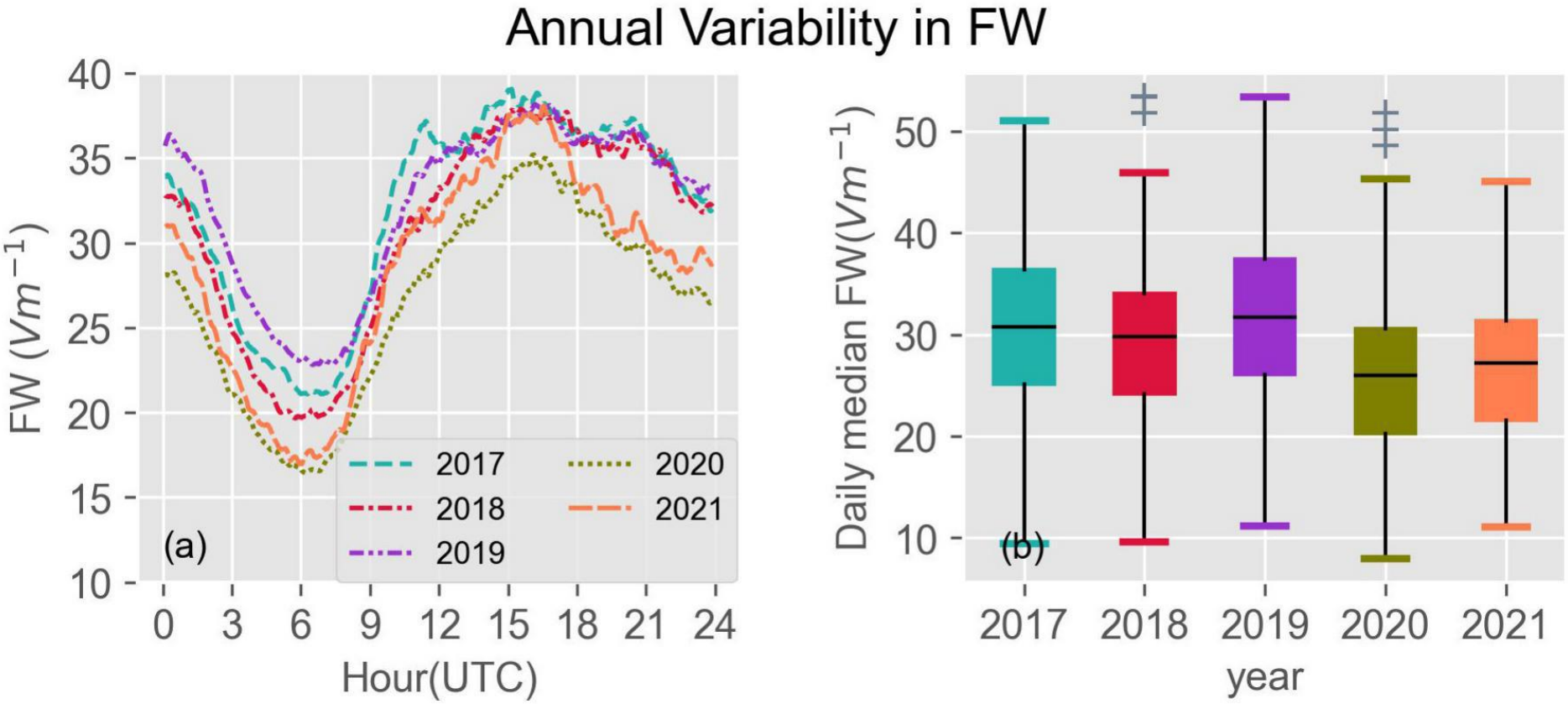
Annual Variability in FW
FW ($Vm^{-1}$)
Hour(UTC)
(a)
2017
2018
2019
2020
2021
Daily median FW($Vm^{-1}$)
year
(b)

Figure 7

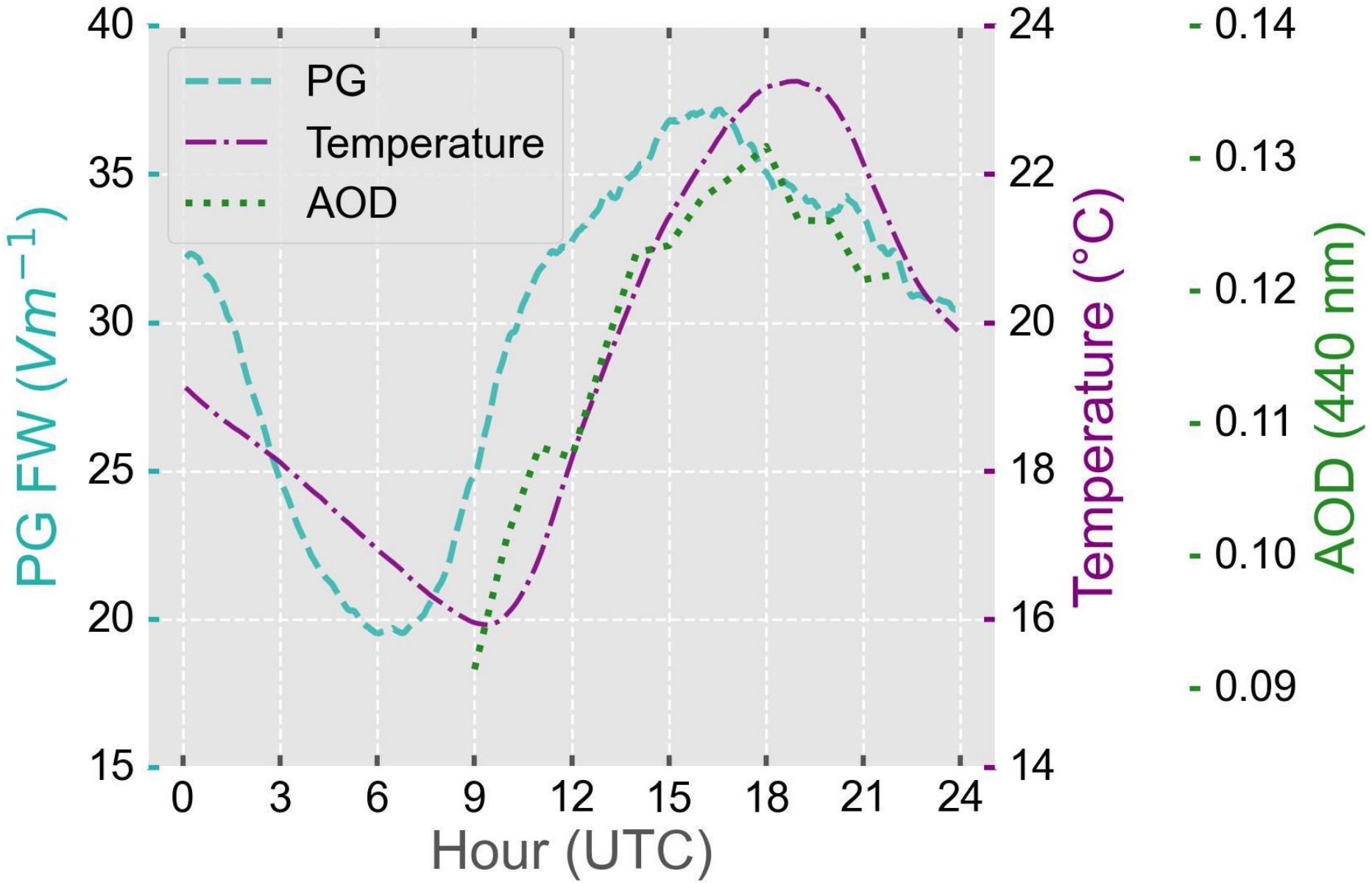
PG
Temperature
AOD
PG FW ($Vm^{-1}$)
Temperature (°C)
AOD (440 nm)
Hour (UTC)
40
35
30
25
20
15
24
22
20
18
16
14
0.14
0.13
0.12
0.11
0.10
0.09
0
3
6
9
12
15
18
21
24

Figure 8

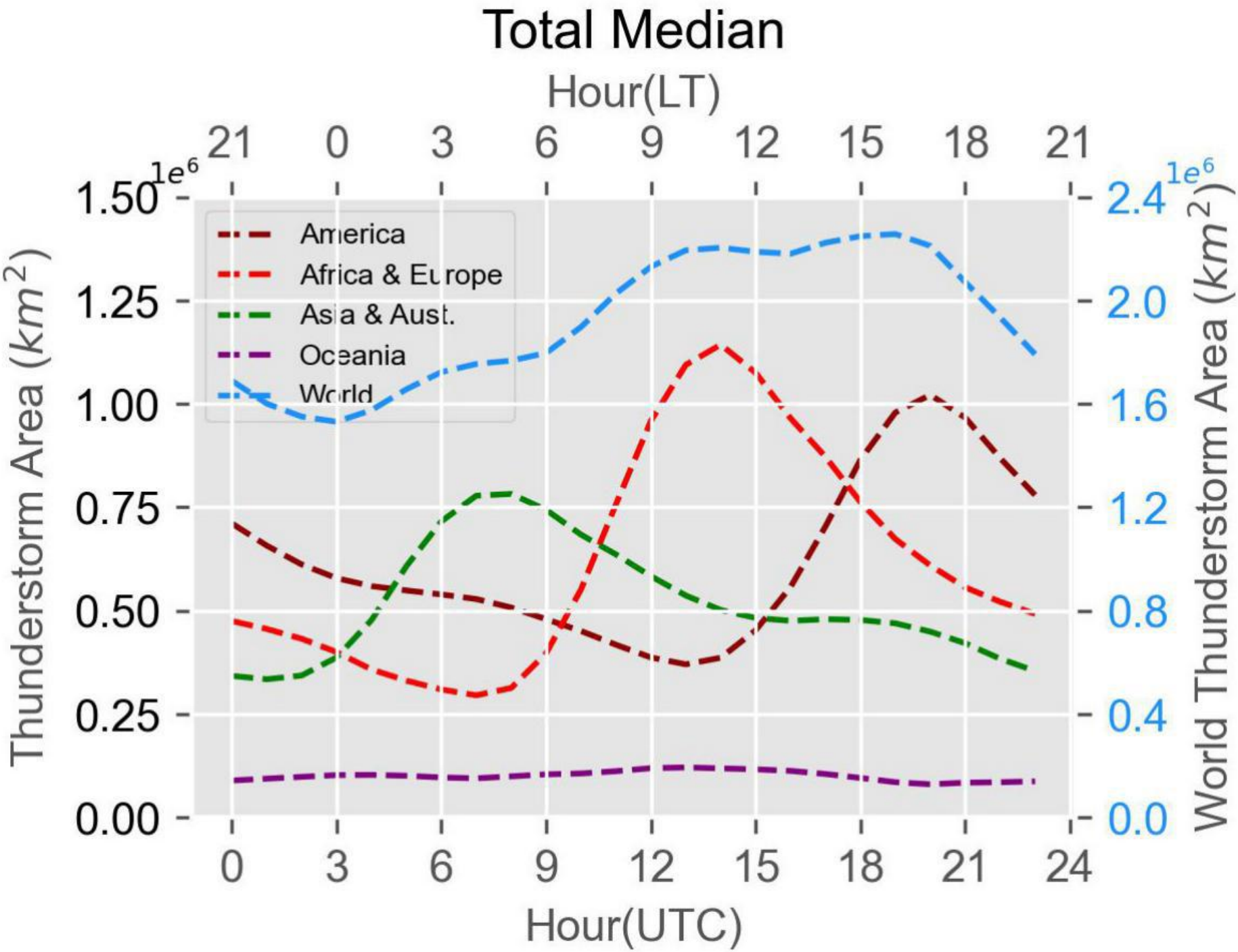
Total Median
Hour(LT)
21 0 3 6 9 12 15 18 21
1e6
1.50
1.25
1.00
0.75
0.50
0.25
0.00
Thunderstorm Area ($km^2$)
America
Africa & Europe
Asia & Aust.
Oceania
World
1e6
2.4
2.0
1.6
1.2
0.8
0.4
0.0
World Thunderstorm Area ($km^2$)
0 3 6 9 12 15 18 21 24
Hour(UTC)

Figure 9

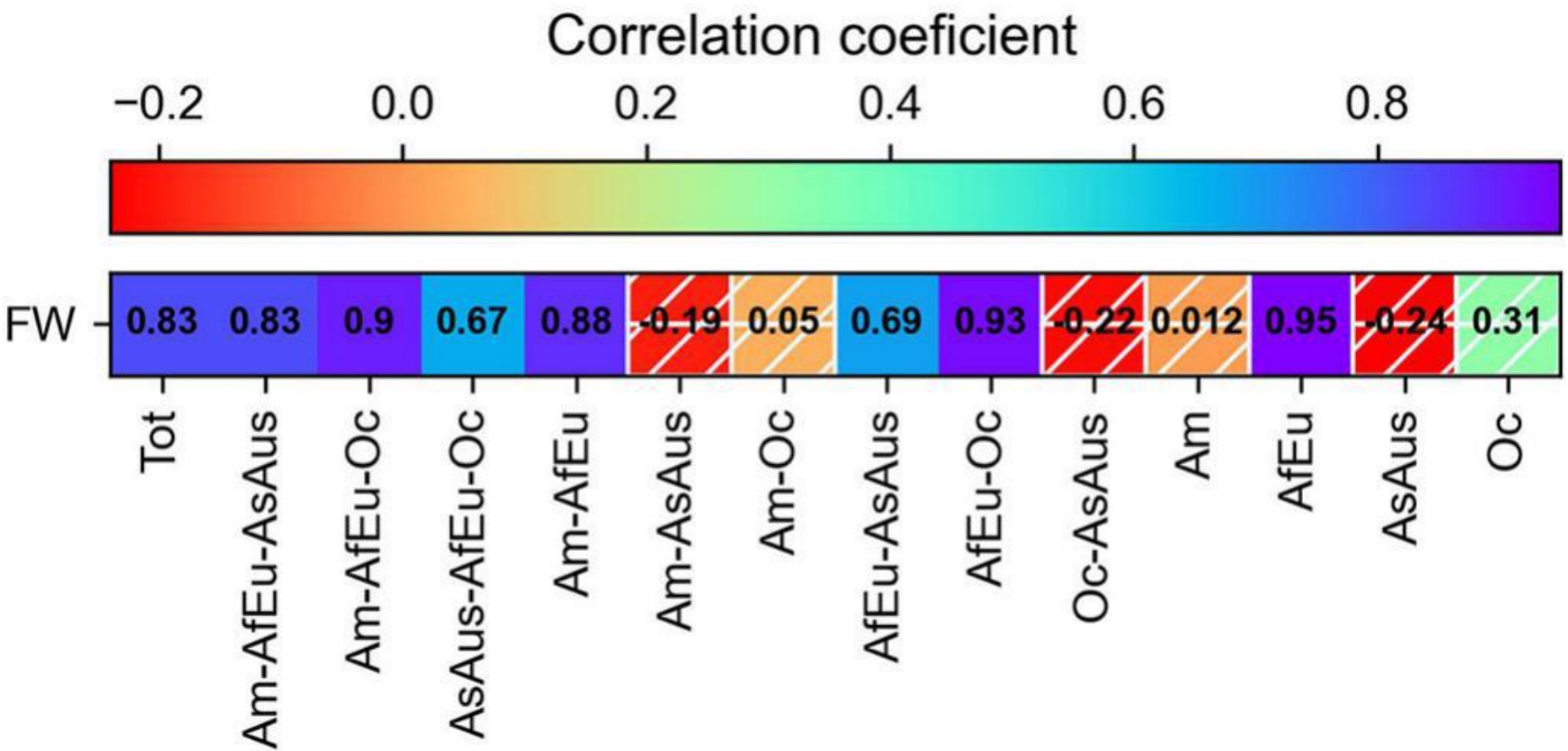
Correlation coeficient
−0.2
0.0
0.2
0.4
0.6
0.8
FW
0.83
0.83
0.9
0.67
0.88
-0.19
0.05
0.69
0.93
-0.22
0.012
0.95
-0.24
0.31
Tot
Am-AfEu-AsAus
Am-AfEu-Oc
AsAus-AfEu-Oc
Am-AfEu
Am-AsAus
Am-Oc
AfEu-AsAus
AfEu-Oc
Oc-AsAus
Am
AfEu
AsAus
Oc

Figure 10

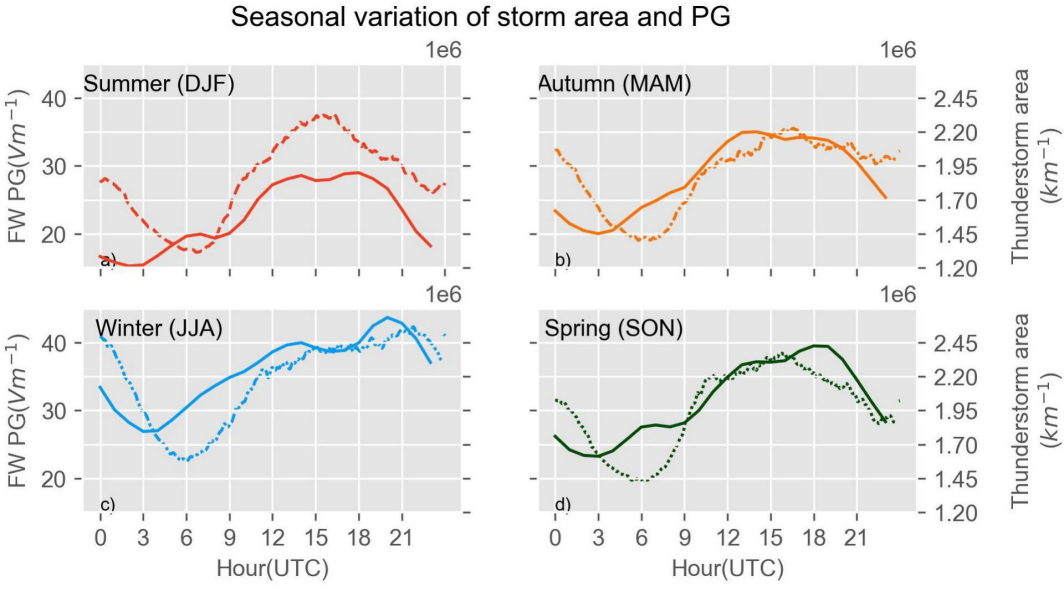
Seasonal variation of storm area and PG
Summer (DJF)
Autumn (MAM)
Winter (JJA)
Spring (SON)
a)
b)
c)
d)
1e6
FW PG($Vm^{-1}$)
Thunderstorm area ($km^{-1}$)
40
30
20
2.45
2.20
1.95
1.70
1.45
1.20
0 3 6 9 12 15 18 21
Hour(UTC)

Figure 11

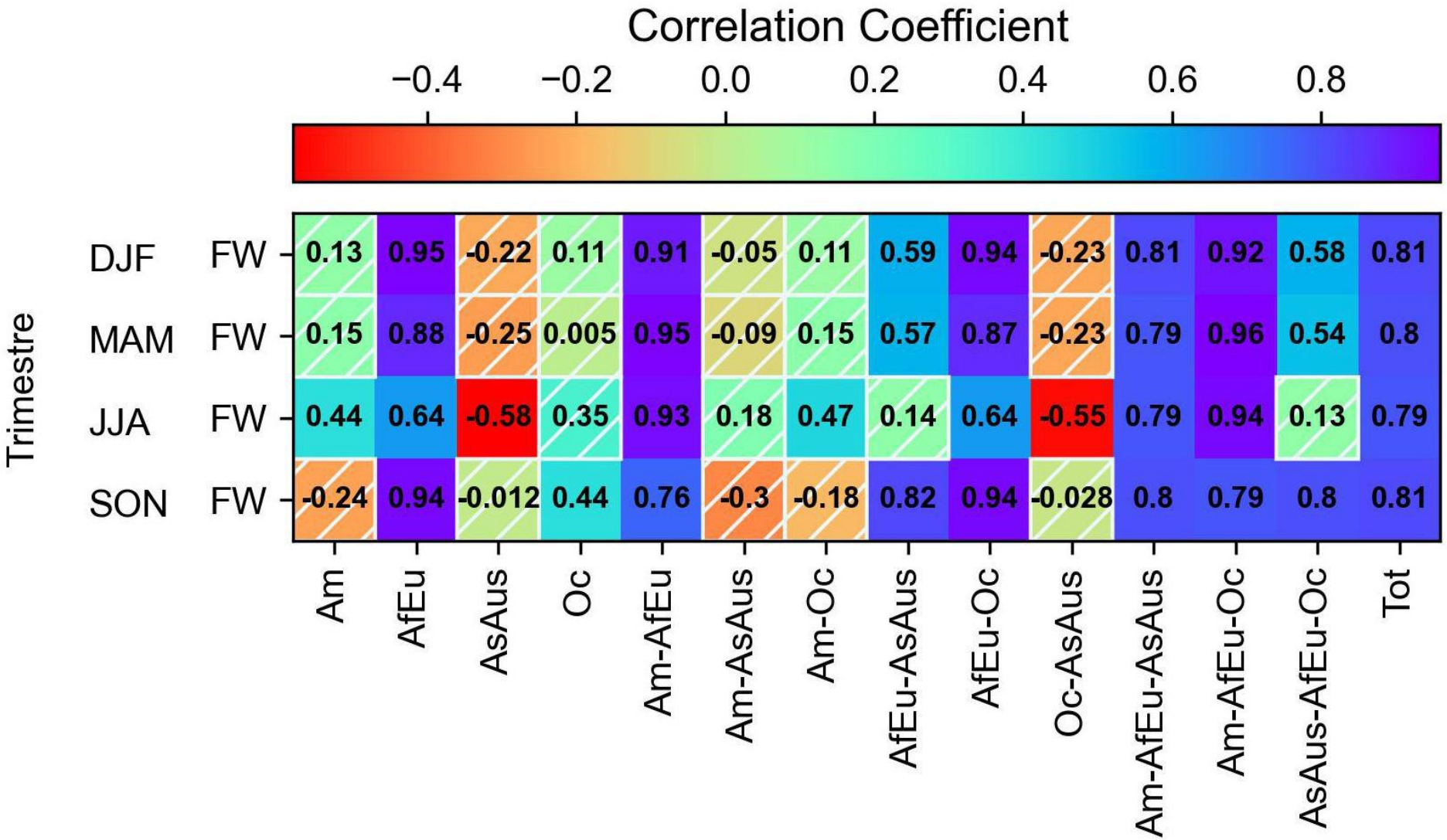
Correlation Coefficient
−0.4
−0.2
0.0
0.2
0.4
0.6
0.8
Trimestre
DJF FW 0.13 0.95 -0.22 0.11 0.91 -0.05 0.11 0.59 0.94 -0.23 0.81 0.92 0.58 0.81
MAM FW 0.15 0.88 -0.25 0.005 0.95 -0.09 0.15 0.57 0.87 -0.23 0.79 0.96 0.54 0.8
JJA FW 0.44 0.64 -0.58 0.35 0.93 0.18 0.47 0.14 0.64 -0.55 0.79 0.94 0.13 0.79
SON FW -0.24 0.94 -0.012 0.44 0.76 -0.3 -0.18 0.82 0.94 -0.028 0.8 0.79 0.8 0.81
Am
AfEu
AsAus
Oc
Am-AfEu
Am-AsAus
Am-Oc
AfEu-AsAus
AfEu-Oc
Oc-AsAus
Am-AfEu-AsAus
Am-AfEu-Oc
AsAus-AfEu-Oc
Tot

Figure 12